J|A|C|S
ARTICLES

Published on Web 04/01/2010

Surface-Initiated Polymerization of Superhydrophobic Polymethylene

Juan C. Tuberquia, Nabijan Nizamidin, Robert R. Harl, Jake Albert, Jason Hunter, Bridget R. Rogers, and G. Kane Jennings*

Department of Chemical and Biomolecular Engineering, Vanderbilt University, Nashville, Tennessee 37235

Received October 9, 2009; E-mail: kane.g.jennings@vanderbilt.edu

Abstract: We report a new surface-initiated polymerization strategy that yields superhydrophobic polymethylene (PM) films from initially smooth substrates of gold and silicon. The films are prepared by assembling a vinyl-terminated self-assembled monolayer, followed by exposure of the surface to a 0.1 M solution of borane, and polymerizing from the borane sites upon exposure to a solution of diazomethane at −17 °C. Surface-initiated polymethylenation (SIPM) presents rapid growth in relation to other surface-initiated reactions, producing PM films thicker than 500 nm after 2 min of reaction and 3 μm after 24 h of reaction. AFM and SEM images show the presence of micro- and nanoscale features that enable the entrapment of air when exposed to water. Consistent with this result, these films exhibit advancing water contact angles greater than 160°, dramatically different than 103° measured for smooth PM films, and hysteresis values ranging from 2° to 40°, depending on the substrate and polymerization time. The superhydrophobic character of the films results in the entrapment of air at the polymer/solution interface to provide remarkable resistances greater than 10^{10} $\Omega \cdot cm^2$ against the transport of aqueous redox probes and cause the film to behave as a "perfect" capacitor.

Introduction

Many innovations in polymer synthesis have been extended to surfaces to create versatile methods for tailoring composition (homopolymers, copolymers),[2,3] modifying architecture (functionalization, hyperbranching),[3,4] and optimizing properties (thickness, density, morphology)[5] of surface-bound polymer films. Some examples of this strategy include the adaptation of solution-phase free radical polymerization,[6,7] ATRP,[8] ROMP,[9] anionic,[10] and cationic[11] reactions into surface-initiated polymerizations. In surface-initiated polymerization (SIP), or "grafting from" methods,[12] an initiator is first immobilized on a surface followed by exposure of the activated surface to an appropriate monomer solution. Activation of the surface is typically attained by self-assembling adsorbates that have the initiator incorporated as the terminus or by modifying a monolayer film to graft the initiator.[12] A completely different SIP approach takes advantage of the catalytic properties of some metal surfaces, since they induce spontaneous polymerization upon exposure to reactive precursors. As an example of this latter method, diazomethane (DM) spontaneously decomposes at gold surfaces to produce linear polymethylene (PM).[13,14] Advantages of using SIP include the preparation of robust, bound coatings over objects of any shape with tailored structure, thicknesses,[12] grafting densities,[12,15] and compositions, including random and block copolymer films.[12,15,16] Here, we adapt the synthetic approach of polyhomologation, developed by Shea and co-workers,[17−20] to prepare surface-initiated polymethylene films with thicknesses exceeding 1 μm on silicon and gold supports.

In their approach, Shea et al.[17−20] react a trialkyl borane initiator in solution with an appropriate ylide monomer, such as dimethylsulfoxonium methylide ($CH_2S(O)Me_2$), to produce end-functionalized polymethylene ($R(CH_2)_nX$ where R and X

(1) Lee, J. K.; Lee, K. B.; Kim, D. J.; Choi, I. S. *Langmuir* **2003**, *19*, 8141–8143.
(2) Bai, D.; Jennings, G. K. *J. Am. Chem. Soc.* **2005**, *127*, 3048–3056.
(3) Bai, D. S.; Ibrahim, Z.; Jennings, G. K. *J. Phys. Chem. C* **2007**, *111*, 461–466.
(4) Zhao, M. Q.; Zhou, Y. F.; Bruening, M. L.; Bergbreiter, D. E.; Crooks, R. M. *Langmuir* **1997**, *13*, 1388–1391.
(5) Huang, W. X.; Kim, J. B.; Bruening, M. L.; Baker, G. L. *Macromolecules* **2002**, *35*, 1175–1179.
(6) Prucker, O.; Ruhe, J. *Macromolecules* **1998**, *31*, 602–613.
(7) Prucker, O.; Ruhe, J. *Macromolecules* **1998**, *31*, 592–601.
(8) Boyes, S. G.; Brittain, W. J.; Weng, X.; Cheng, S. Z. D. *Macromolecules* **2002**, *35*, 4960–4967.
(9) Weck, M.; Jackiw, J. J.; Rossi, R. R.; Weiss, P. S.; Grubbs, R. H. *J. Am. Chem. Soc.* **1999**, *121*, 4088–4089.
(10) Jordan, R.; Ulman, A.; Kang, J. F.; Rafailovich, M. H.; Sokolov, J. *J. Am. Chem. Soc.* **1999**, *121*, 1016–1022.
(11) Jordan, R.; Ulman, A. *J. Am. Chem. Soc.* **1998**, *120*, 243–247.
(12) Jennings, G. K.; Brantley, E. L. *Adv. Mater.* **2004**, *16*, 1983–1994.
(13) Guo, W. F.; Jennings, G. K. *Langmuir* **2002**, *18*, 3123–3126.
(14) Seshadri, K.; Atre, S. V.; Tao, Y. T.; Lee, M. T.; Allara, D. L. *J. Am. Chem. Soc.* **1997**, *119*, 4698–4711.
(15) Ruckenstein, E.; Li, Z. F. *Adv. Colloid Interface Sci.* **2005**, *113*, 43–63.
(16) Edmondson, S.; Osborne, V. L.; Huck, W. T. S. *Chem. Soc. Rev.* **2004**, *33*, 14–22.
(17) Shea, K. J.; Staiger, C. L.; Lee, S. Y. *Macromolecules* **1999**, *32*, 3157–3158.
(18) Shea, K. J.; Walker, J. W.; Zhu, H.; Paz, M.; Greaves, J. *J. Am. Chem. Soc.* **1997**, *119*, 9049–9050.
(19) Busch, B. B.; Paz, M. M.; Shea, K. J.; Staiger, C. L.; Stoddard, J. M.; Walker, J. R.; Zhou, X. Z.; Zhu, H. D. *J. Am. Chem. Soc.* **2002**, *124*, 3636–3646.
(20) Busch, B. B.; Staiger, C. L.; Stoddard, J. M.; Shea, K. J. *Macromolecules* **2002**, *35*, 8330–8337.

Scheme 1. Mechanism of Reaction between a Trialkylborane and Dimethylsulfoxonium Methylide to Prepare Polymethylene Chains

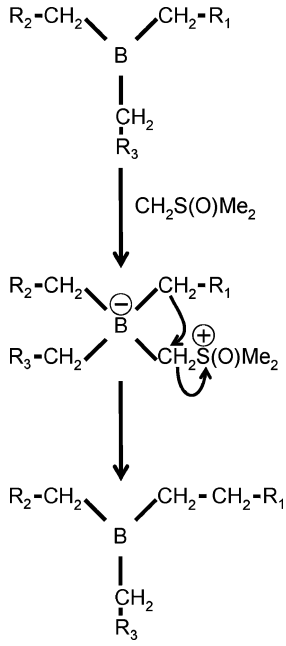

are various terminal groups). Scheme 1 shows the polyhomologation mechanism. In this mechanism the three alkyl groups of the initiator have the same probability to undergo a 1,2 migration, resulting in a low polydispersity product that reacts with additional ylide to extend the chain length.[17] Oxidation with basic peroxide[18] or trimethylamine *N*-oxide dehydrate[21] produces an alcohol-terminated polymethylene that can be converted to various functional groups (X).[18] The terminal R-group at the opposite end of the chain is introduced by reacting an R-terminated olefin with diborane (B_2H_6) prior to reaction with the ylide in Scheme 1. The primary advantages of polyhomologation[18,20] are the low polydispersity of the polymer (1.04−1.17), the rapid kinetics of polymerization, and the tight control over the molecular weight by varying the ratio of ylide to trialkylborane.

Here, we develop a surface-initiated polymethylenation (SIPM) to grow polymethylene films from borane-modified gold or silicon surfaces by exposure to dilute diazomethane in ether at −17 °C. Scheme 2 presents our strategy for polymerizing over immobilized monoalkylborane sites on gold and silicon substrates. First, we prepare a vinyl-terminated monolayer on the substrate.[22] Then, the initiator is immobilized on the surface by hydroborating the vinyl termini in a solution of borane (BH_3) in tetrahydrofuran (THF) under inert atmosphere. Immersion of the functionalized surface into a dilute DM solution enables polymerization from the borane centers, yielding a PM film.[23,24] Exposure of unmodified gold surfaces to DM also produces a PM film due to spontaneous polymerization at gold surface sites.[14] To isolate the effect of the monoalkylborane initiation sites on the gold surface in our process, we predeposit a silver

Scheme 2. Strategy for the Polymethylenation of Diazomethane at Heterogeneous Borane Sites on Gold with and without a Monolayer of Silver, and Silicon Surfaces[a]

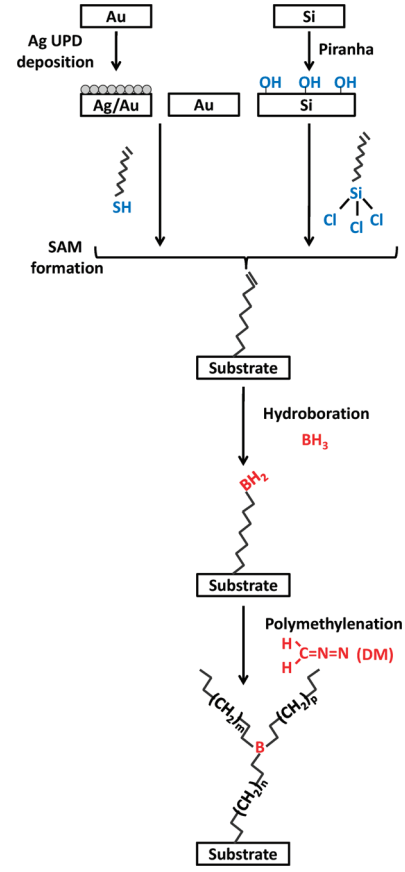

[a] A vinyl-terminated monolayer is exposed to a 0.1 M solution of borane in THF, followed by exposure to a DM solution in ether at −17 °C. The silver layer on gold prevents the spontaneous polymerization of DM into PM that is observed on gold.

monolayer on the gold surface to greatly inhibit the spontaneous growth of PM films.[13,25]

The spontaneous growth of ultrathin PM films on gold has been the subject of previous studies[2,14,25] that take advantage of the low cost, chemically inert character, and low dielectric constant of PM[26] to prepare ultrathin polymer films and overcome limitations of PM processability due to poor solubility in organic solvents[27] and poor adhesion to metal substrates[28] that limit spin coating and solution casting. Seshadri et al.[14] grew ∼50 nm PM films by exposing gold surfaces to a DM solution in ether. Our group[13,25] developed approaches to enhance or prevent PM growth by atomically modifying gold surfaces with copper or silver, respectively. Different surfaces[29−31] also favor DM decomposition to form PM. However, polymerization by these routes relies on the inherent catalytic properties of the substrate. Using SIPM, we intend to expand the initiation capabilities of boranes to noncatalytic surfaces, thus diversifying the number of substrates from which PM films can be grown.

(21) Wagner, C. E.; Rodriguez, A. A.; Shea, K. J. *Macromolecules* **2005**, *38*, 7286–7291.
(22) Peanasky, J. S.; McCarley, R. L. *Langmuir* **1998**, *14*, 113–123.
(23) Davies, A. G.; Hare, D. G.; Khan, O. R.; Sikora, J. *J. Am. Chem. Soc.* **1963**, 4461–4471.
(24) Davies, A. G.; Hare, D. G.; Khan, O. R.; Sikora, J. *Proc. Chem. Soc.* **1961**, 172.
(25) Guo, W. F.; Jennings, G. K. *Adv. Mater.* **2003**, *15*, 588–591.
(26) James, M. *Polymer Data Handbook*; Oxford University Press: New York, 1999.
(27) Brandrup, J.; Immergut, E. H.; Grulke, E. A.; Abe, A.; Bloch, D. R. In *Polymer Handbook*; Wiley & Sons: New York, 1999.
(28) Kong, J.-S.; Lee, D.-J.; Kim, H.-D. *J. Appl. Polym. Sci.* **2001**, *82*, 1677–1690.
(29) Lie, L. H.; Patole, S. N.; Hart, E. R.; Houlton, A.; Horrocks, B. R. *J. Phys. Chem. B* **2002**, *106*, 113–120.

In this article, we report the first surface-initiated polymethylenation for the growth of PM films from gold and silicon surfaces. This surface reaction is rapid in comparison to many surface-initiated polymerizations, producing PM films thicker than 500 nm after 2 min of reaction and 3 μm after 24 h of reaction. Extremely high contact angles (>160°) and low hystereses (~2°) indicate that PM films exhibit superhydrophobic behavior due to their low surface energy and their combination of micrometer- and nanoscale morphology. Thus, our approach modifies a smooth substrate into a rough, superhydrophobic surface through a single polymerization step. Due to the presence of entrapped air at the water/polymer interface, these superhydrophobic films present large resistances on the order of 1×10^{10} $\Omega \cdot cm^2$ against the transport of aqueous redox probes.

Results and Discussion

Characterization of Surface Borane. Hydroboration of olefins in solution results in trialkylboranes, except in the case of sterically hindered olefins, in which hydroboration yields dialkylboranes or monoalkylboranes.[32,33] Here, we exposed a dense vinyl-terminated monolayer to a solution of borane in THF. The immobilization of the chains within the monolayer prevents the formation of trialkylboranes, and further, the formation of dialkylboranes that would require chain termini to be within ~3 Å based on the C−B bond length[34] and the geometry of the binding is unlikely on average, given the ~5 Å center-to-center distance between chains in an alkanethiolate monolayer.[35] Therefore, we deduce that the exposure of a vinyl-terminated monolayer to borane results predominately in a monoalkylborane and a $-BH_2$ terminus. However, characterization of the monoalkylborane self-assembled monolayer (SAM) is challenging because our primary surface characterization methods (PM-IRRAS, XPS, etc.) require the surfaces to be exposed to air, and alkyl boranes are known to react rapidly with oxygen in the air to yield a variety of oxidized species.[36−38] Our approach was to preoxidize[39] the surface prior to characterization. Therein, we exposed a freshly hydroborated vinyl-terminated monolayer on gold to O_2-saturated THF for 1 h and water for 30 min (denoted as HBO) before exposure to air for subsequent characterization with PM-IRRAS and XPS.

Figure 1 shows the IR and the XPS spectra of an HBO surface and a vinyl-terminated SAM (C═C/Au) that were each exposed to the same oxidizing conditions. The IR spectrum of the vinyl-terminated SAM displays the C−H out-of-plane deformation (912 cm^{-1}) and the out-of-plane deformation of the C═C (993 cm^{-1}) groups characteristic of the vinylic bond.[22,40,41] The spectrum for the HBO monolayer shows a disappearance of the C═C modes, consistent with hydroboration of the vinyl functionality at the surface of the monolayer, and the appearance of a peak at 1264 cm^{-1} that we assign to symmetric B−O stretching,[42,43] suggesting the subsequent oxidation of $B-H_2$ bonds to $B-(OH)_2$ (boronic acid).[32,34,38,39] Orientation of the B−OH groups at the outer surface would result in a dominant symmetric B−O stretch, based on surface selection rules,[44] as compared to the more commonly observed asymmetric B−O stretch,[45,46] which we do not observe here. Higher reactivity of the H−B bond toward O_2 as compared to the B−C bond could result from the confinement of the latter within the SAM, which lowers its exposure and increases the steric hindrance toward oxidation.[47,48]

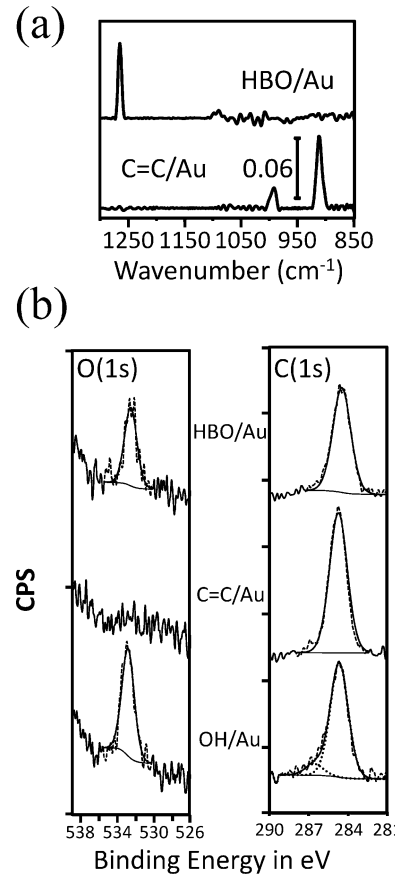

Figure 1. (a) PM-IRRAS spectrum of a hydroborated SAM after its oxidation with pure oxygen (HBO) for 1 h and immersion in water for 30 min. For comparison a spectrum for a vinyl-terminated SAM exposed to the same conditions (C═C/Au) is also displayed. Modulation was focused in the lower (1129 cm^{-1}) region of the spectra. (b) XPS spectra for a hydroborated (HBO) and a vinyl-terminated (C═C/Au) SAM after exposure to oxidation conditions. Spectrum of a hydroxyl-terminated monolayer (OH/Au) is presented for comparison. The suvey XPS spectra (not shown) confirm the presence of Au, C, O, and S on all surfaces except for the absence of O on the vinyl-terminated monolayer. Spectra have been offset for clarity.

(30) Kubota, H.; Morawetz, H. *J. Polym. Sci. Part A-1: Polym. Chem.* **1967**, *5*, 585–591.
(31) Bart, J. C.; Cariati, F.; Erre, L.; Gessa, C.; Micera, G.; Piu, P. *Clays Clay Miner.* **1979**, *27*, 429–432.
(32) Brown, H. *Boranes in Organic Chemistry*; Cornell University Press: Ithaca, 1972.
(33) Brown, H. C.; Rao, B. C. S. *J. Am. Chem. Soc.* **1959**, *81*, 6428–6434.
(34) Onak, T. *Organoborane Chemistry*; Academic Press: New York, 1975.
(35) Ulman, A. *Chem. Rev.* **1996**, *96*, 1533–1554.
(36) Mirviss, S. B. *J. Am. Chem. Soc.* **1961**, *83*, 3051–3056.
(37) Mirviss, S. B. *J. Org. Chem.* **1967**, *32*, 1713.
(38) Davies, A. G. *J. Chem. Res.-Synop.* **2008**, 361–375.
(39) Brown, H. C.; Midland, M. M. *Tetrahedron* **1987**, *43*, 4059–4070.
(40) Snyder, R. G.; Strauss, H. L.; Elliger, C. A. *J. Phys. Chem.* **1982**, *86*, 5145–5150.
(41) Sulc, R.; Zhou, X. Z.; Shea, K. J. *Macromolecules* **2006**, *39*, 4948–4952.
(42) Shurvell, H. F.; Faniran, J. A. *Can. J. Chem.* **1968**, *46*, 2082.
(43) Faniran, J. A.; Shurvell, H. F. *Can. J. Chem.* **1968**, *46*, 2089.
(44) Bradshaw, A. M.; Richardson, N. V. *Pure Appl. Chem.* **1996**, *68*, 457–467.
(45) Barriet, D.; Yam, C. M.; Shmakova, O. E.; Jamison, A. C.; Lee, T. R. *Langmuir* **2007**, *23*, 8866–8875.
(46) Brewer, S. H.; Allen, A. M.; Lappi, S. E.; Chasse, T. L.; Briggman, K. A.; Gorman, C. B.; Franzen, S. *Langmuir* **2004**, *20*, 5512–5520.
(47) Brown, H. C.; Dodson, V. H. *J. Am. Chem. Soc.* **1957**, *79*, 2302–2306.

To provide an estimate of boron surface coverage on the HBO monolayer, we used X-ray photoelectron spectroscopy (XPS). Figure 1b shows the C(1s) and O(1s) high-resolution spectra for the HBO monolayer, the vinyl-terminated monolayer, and a hydroxyl-terminated monolayer (OH/Au) prepared from $HS(CH_2)_{11}OH$ on Au. These spectra show that all monolayers exhibit the characteristic C(1s) peak for aliphatic hydrocarbons at 284.7 eV. The spectrum for the hydroxyl-terminated monolayer exhibits a shoulder at 286.8 eV corresponding to the outermost carbon that is covalently bound to the oxygen of the hydroxyl group.[49] The atomic concentration ratio of these two peaks is 10:1, consistent with the chain length of the hydroxyl monolayer. Appearance of a single and sharp peak for the HBO monolayer indicates the absence of the C−O bond, suggesting that the oxygen present in the system is not bonded to carbon, but most likely to boron. Direct detection of boron was not observed due to its low atomic concentration (≤1 B:11 C) and small sensitivity factor, ~20% of that for oxygen.[50] Instead, we used the presence of oxygen in the spectra as indirect evidence of an oxidized boron functionality. Importantly, high-resolution spectra of the O(1s) region indicate the presence of oxygen on the HBO surface but not on the vinyl-terminated control. On the basis of a comparison of the atomic ratios of O to C in both the HBO and OH-terminated monolayers, we estimate that the oxygen level on the HBO surface is 70 ± 9% of that on a dense HO-terminated SAM. Since boronic acids dehydrate in vacuum to form boroxine glasses with a stoichiometry of one oxygen per boron,[51] we assume that our oxidized species has one oxygen per boron per chain, yielding an estimate of boron surface coverage of 70 ± 9% from XPS. As further evidence of the presence of boron, exposure of the HBO surface on silicon to diazomethane in ether results in a PM film (vide infra) that is ~35% as thick as a film grown from an unoxidized HB monolayer, consistent with the presence of a boron functionality within the monolayer after oxidation since a nonhydroborated vinyl monolayer on silicon yields no polymer.

On silicon substrates, the abundance of oxygen in the native oxide layer hindered our ability to use XPS to detect oxygen levels in the monolayer as an estimate of boron coverage. Instead, we incorporated the approach of Wasserman et al.[52] to completely oxidize the surface boranes to hydroxyl groups by exposure to a 0.2 N solution of NaOH in H_2O_2 (30%) for 12 h under inert atmosphere.[53] Wasserman et al.[52] used this approach to estimate the conversion of vinyl groups to a hydroxyl functionality. We observed that this harsh oxidation destroys thiolate SAMs but does not damage the more robust siloxane-linked monolayers on silicon. Exposure of the H_2B-termini to the oxidizing conditions resulted in an advancing water contact angle (θ_{HB}) of 53°, whereas a vinyl-terminated control was not affected by the conditions as the contact angle ($\theta_{C=C}$) remained 95°. Calculations of yield were performed using the Cassie equation,[52]

$$\cos\theta_{HB} = \phi_{C=C}\cos\theta_{C=C} + \phi_{OH}\cos\theta_{OH} \quad (1)$$

Table 1. Thickness Measurements for PM Films Grown from the Indicated Surfaces upon Exposure to a 13 mM Solution of DM in Ether at −17 °C for 24 h

substrate	ellipsometry, nm	QCM, nm	profilometry, nm
HB+Au		3608	3500 ± 200
SAM+Au	363 ± 12	238	344 ± 15
HB+Ag/Au		3006	
SAM+Ag/Au	1 ± 0.1		
Ag/Au	6 ± 3		
Au	224 ± 1	182	277 ± 5
HB+Si			1667 ± 190
SAM+Si	1 ± 0.2		

where $\phi_{C=C}$ and ϕ_{OH} are the surface area fractions of the vinyl- and hydroxyl-terminations in contact with water, respectively. Assuming $\theta_{OH} \approx 0°$, the final monolayer exhibits a higher surface energy as compared to the initial vinyl-terminated monolayer and indicates that ~35% of the surface area presents the vinyl termini ($\phi_{C=C}$) and 65% represents hydroxyl termini (ϕ_{OH}) from the direct conversion of surface boranes. This result on silicon is in good agreement with XPS results on gold and suggests that after hydroboration ~65% of the vinyl-termini are converted to H_2B-terminations through the hydroboration step.

Effect of Substrate. To investigate the effect of hydroboration on the surface-initiated growth of PM, we measured the thicknesses of PM films grown from hydroborated surfaces and control substrates upon exposure to a 13 mM solution of DM in ether at −17 °C for 24 h. Table 1 shows the results of the thickness measurements for PM films grown from six surfaces, including two hydroborated SAMs, one on gold (HB+Au) and another on Ag/Au UPD (HB+Ag/Au); two vinyl-terminated SAMs not exposed to borane (SAM+Au, SAM+Ag/Au), as well as bare Au and Ag/Au surfaces. In principle, ellipsometric measurements were performed on all the films, assuming that they are uniform and isotropic and have the same refractive index as polyethylene ($n = 1.5$).[27] All the control films could be fit with a Cauchy model to determine their thickness, but PM films grown from hydroborated SAMs could not be fit with this simple model, perhaps due to their rough morphology (vide infra). To assess the rough morphology of the surface, we used an effective medium approximation[54] model that combined the optical constants for PM and air. However, this approach did not provide a good fitting of the experimental data. This characteristic behavior suggests that PM films grown from SIPM are distinct in comparison to the control films. To provide a measure of thickness for these rougher PM films, we performed profilometry and ex situ quartz crystal microgravimetry (QCM) measurements.[14]

To verify the validity of profilometry and QCM, we first compared the results for a PM film on Au with those from ellipsometry to determine if the techniques are in relative agreement. Comparison of the thickness values for PM growth on Au and SAM+Au surfaces obtained by QCM, ellipsometry, and profilometry shows that QCM-estimated thicknesses are ~25% lower than the average of the three techniques. However, the fact that, in all cases, PM films grown from SAM+Au present much higher thicknesses as compared to those grown

(48) Mikhailov, B. M.; Bubnov, Y. *Organoboron Compounds in Organic Synthesis*; Harwood Academic: New York, 1984.
(49) Bain, C. D.; Troughton, E. B.; Tao, Y. T.; Evall, J.; Whitesides, G. M.; Nuzzo, R. G. *J. Am. Chem. Soc.* **1989**, *111*, 321–335.
(50) Ulvac-PHI, Inc. *Operator's PHI Multipak software manual*, version 8.2C; Ulvac-PHI, Inc.: Chigasaki City, Kanagawa Prefecture, Japan, 2007.
(51) Carey, R. I.; Folkers, J. P.; Whitesides, G. M. *Langmuir* **1994**, *10*, 2228–2234.
(52) Wasserman, S. R.; Tao, Y. T.; Whitesides, G. M. *Langmuir* **1989**, *5*, 1074–1087.
(53) Faucheux, N.; Schweiss, R.; Lutzow, K.; Werner, C.; Groth, T. *Biomaterials* **2004**, *25*, 2721–2730.
(54) Guide to using WVASE32 Software for spectroscopic ellipsometry data acquisition and analysis, Version 3.335; J.A. Woollam Co., Inc., 2001.

from Au indicates that the techniques certainly agree with respect to the overall trend.

Table 1 shows that SIPM allows the growth of films that are 10- to 1000-fold thicker than films grown from non-hydroborated substrates. In fact, the ~3 μm thick films produced by SIPM are among the thickest films yet reported by surface-initiated routes. From the evaluation of the non-hydroborated surfaces, we notice that silver deposition on gold surfaces (Ag/Au and SAM+Ag/Au) inhibits spontaneous PM formation, as previously described by our group.[13,25] This inhibition indicates that the PM film grown on the HB+Ag/Au surface results from SIPM and not from spontaneous polymerization. In the case of the HB+Au surface, SIPM produces a film about 10 times thicker than the thickest non-hydroborated PM film (SAM+Au), supporting the dominance of SIPM toward film growth when both SIPM and spontaneous[14] modes are present.

Table 1 also shows the thicknesses obtained after exposure of DM at the above conditions to a silicon substrate modified by 5-hexenyltrichlorosilane (SAM+Si) and one that was further modified by borane (HB+Si). While PM does not grow on SAM-modified silicon, as evidenced by a thickness that is approximately that of the SAM, it does grow from HB+Si to achieve a thickness that is 55% of that for SIPM from HB+Ag/Au after 24 h of polymerization. We did observe that HB+Si requires longer times of polymerization to obtain comparable thicknesses to those obtained for shorter times on HB+Ag/Au and HB+Au. The slower polymerization on silicon could result from a greater extent of oxidation of this monolayer during transfer of the substrate into the DM solution for polymerization. As the 6-carbon vinyl-terminated monolayer on silicon is thinner and less crystalline than the 11-carbon monolayer on Au and Ag/Au,[55] the C−B bond within the monolayer on silicon is more exposed and, thus, more susceptible to attack by oxygen. Insertion of oxygen into the C−B bond would result in a lower number of C−B bonds that enable the polymerization. Appreciable differences in the reactivity of various boranes toward DM was reported by Davies et al.[23] in which the polymerization of PM by alkylboranes is faster as compared to that of oxidized states: $R_3B > (RBO)_3 > (R_2B)_2O > RB(OR)_2 > (RO)_3B$. Nonetheless, growth of PM films from HB+Si demonstrates the ability to extend SIPM to other vinyl-terminated substrates. For PM films grown from HB+Ag/Au and HB+Au surfaces, discrepancies in their thicknesses result from the catalytic activity of Au toward DM, resulting in slightly thicker films.

Effect of Concentration and Time. Figure 2 shows the effect of the time of polymerization and the concentration of DM on the PM film thickness on HB+Ag/Au substrates. Figure 2a shows the variation of film thickness measured by profilometry at various times of polymerization after exposure to a 15 mM solution of DM at −17 °C. The films achieve thicknesses of ~1 μm after 10 min of reaction, presenting rapid kinetics as compared to other SI routes.[13,14] The growth rate slows as the reaction proceeds, suggesting occlusion of monomers to the active borane sites. Figure 2b shows the effect of DM concentration on the growth of PM films after 24 h of exposure to DM solutions with concentrations between 0.2 and 15 mM at −17 °C. Film thickness increases sharply with concentration from 0 to 1 mM with a moderate dependence for higher concentrations. Figure 2b shows that films with thicknesses greater than 1 μm can be grown in 24 h if the concentration of DM is greater than 1 mM.

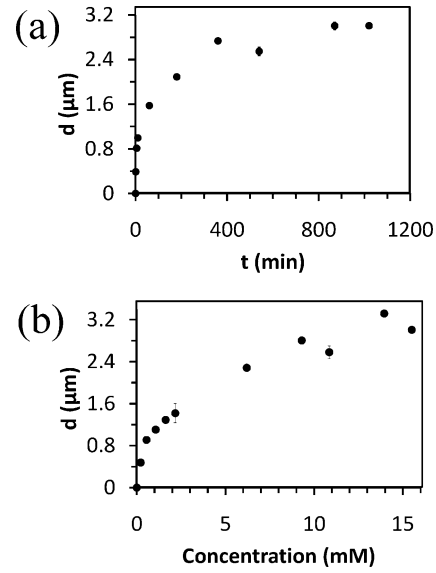

Figure 2. Thickness of PM films grown from HB+Ag/Au surfaces as affected by (a) time of polymerization after exposure to a 15 mM solution of DM at −17 °C and (b) DM concentration (0.2 to 15 mM) after 24 h of reaction at −17 °C. The data points and error bars represent the averages and standard deviations, respectively, of measurements obtained on two samples prepared independently.

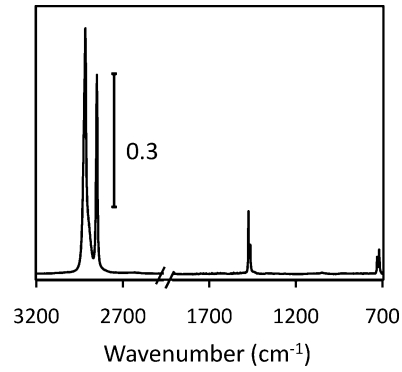

Figure 3. RAIR spectrum for a PM film after 1 h of polymerization in a 8.5 mM solution of DM in ether for 1 h.

Film Composition and Structure. We used RAIRS to assess the composition and structure of polymer films grown by SIPM and enable comparison with PM films formed by spontaneous polymerization (controls) that have been characterized previously.[14,25] We first exposed a HB+Au surface to an 8.5 mM solution of DM in ether for 1 h. RAIR spectra of the film (Figure 3) show the relevant regions of PM: CH_2 stretching[40,41] (ν_{as} = 2918 cm^{-1}, ν_s = 2850 cm^{-1}), CH_2 bending[13,14,56] (ν_{as} = 1473 cm^{-1}, ν_s = 1463 cm^{-1}), and CH_2 rocking modes[13,14,56,57] (split: ν_{as} = 730 cm^{-1} and ν_s = 720 cm^{-1}). The positions of these modes are consistent with crystalline PM chains, and the absence of methyl modes in the IR spectra at 2960 and 2880 cm^{-1} indicates the linear character of the PM chains.[2]

To further evaluate the structure of PM films, we exposed the same six substrates listed in Table 1 to a 13 mM solution of DM in ether for 24 h and collected RAIR spectra. Figure 4 shows the relevant regions of the RAIR spectra for CH_2 bending[13,14,56] and CH_2 rocking modes.[13,14,56,57] Comparison

(55) Brunner, H.; Vallant, T.; Mayer, U.; Hoffmann, H. *Surf. Sci.* **1996**, *368*, 279–291.

(56) Colthup, N.; Daly, L.; Wiberley, S. *Introduction to Infrared and Raman Spectroscopy*, 3rd ed.; Academic Press: Boston, 1990.

(57) Snyder, R. G. *J. Chem. Phys.* **1979**, *71*, 3229–3235.

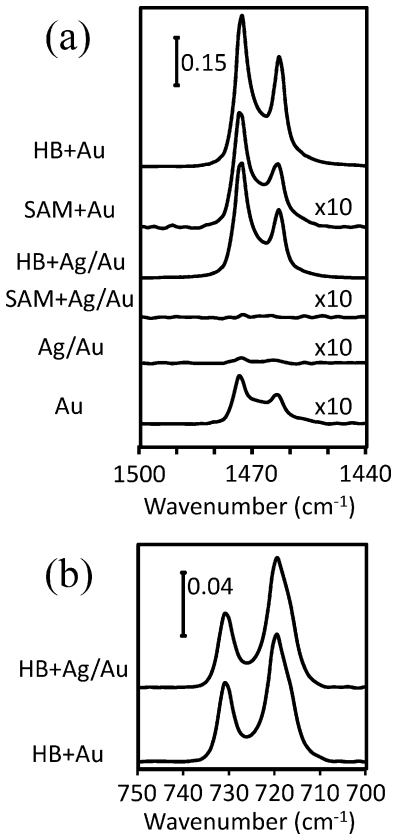

Figure 4. RAIR spectra for PM films grown by exposure to a 13 mM solution of DM in ether for 24 h. (a) CH bending region of PM films grown from the same six substrates listed in Table 1, with four of the spectra multiplied by 10 to enable comparison with spectra for thicker PM films grown from HB+Au and HB+Ag/Au. (b) CH rocking region for PM films grown from Ag/Au and Au surfaces. The spectra have been offset vertically for clarity.

of the RAIR peak absorbance (Figure 4a) for the various surfaces supports thickness measurements and shows that SIPM enables the formation of PM films. Figure 4 also provides information on the structure and conformation of PM films on HB+Au and HB+Ag/Au surfaces. Figure 4a shows the CH bending region for PM films on HB+Ag/Au and HB+Au. The split character of the peak into asymmetric ($\nu_{as} = 1473$ cm^{-1}) and symmetric ($\nu_s = 1463$ cm^{-1}) modes indicates that there are two types of chain configurations in the unit subcell,[58] a prime characteristic of orthorhombic chain packing. In agreement with the orthorhombic conformation, the CH rocking mode also splits into in-phase and out-of-phase modes[14] at 731 and 719 cm^{-1} (Figure 4b), respectively. If we assume that the orthorhombic conformation is the only crystalline structure present and the rest of the chains have no conformational order,[14] we can estimate an orthorhombic crystalline content of ~70% for the HB+Au and HB+Au/Ag surfaces. This calculation uses the theoretical consideration for paraffins where the ratio of the rocking intensities $I_{720}/I_{730} = 1.233$.[57] Spectra (not shown) obtained after exposure of a HB+Si surface to a 13 mM solution of DM in ether at −17 °C for 24 h are similar to those shown in Figure 4.

Surface Topography. Figure 5 shows scanning electron microscopy (SEM) images to reveal the distinctive topographical features for PM films grown from HB+Si, HB+Au, and

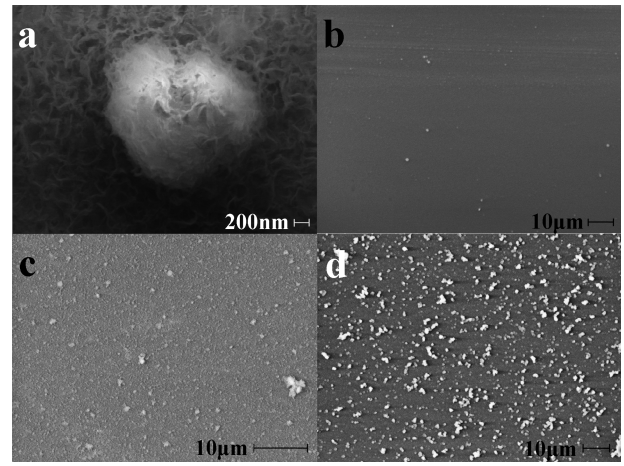

Figure 5. Scanning electron microscopy of PM films grown from HB+Si (a, b), HB+Ag/Au (c), and HB+Au (d) upon exposure to a 13 mM solution of DM in ether at −17 °C for 24 h.

HB+Ag/Au surfaces after 24 h of reaction in a 13 mM solution of DM in ether at −17 °C. Figure 5a presents a PM film grown from HB+Si showing nanometer-scale ridges and valleys and a micrometer-scale cluster that is characteristic of PM films grown from SIPM. Comparison of PM films grown from HB+Si, HB+Ag/Au, and HB+Au surfaces (Figure 5b, c, and d) shows that the main topographical difference of the three substrates is related to the concentration of the micrometer-scale clusters, with films grown from HB+Si providing the least concentrated clusters on the surface and those on HB+Au the most concentrated clusters. To confirm that PM clusters result from the SIPM, we compared SEM images for films with no additional treatment after extraction from the DM solution and films that were vigorously rinsed with trichlorobenzene and ethanol after polymerization. Rinsing the films removed some large agglomerates (>5 μm in diameter), but the ~1 μm PM clusters remained firmly attached to the surface. These clusters survive AFM scanning (see Figure 6), and their mountain-like morphology (Figure 5a or 6a) suggests they are produced from the surface-initiated polymerization.

Finally, to more accurately determine the dimensions of the topographical features of PM films via SIPM, Figure 6 presents an atomic force microscopy (AFM) 3D representation of the HB+Au surface after 24 h of reaction in a 13 mM solution of DM in ether at −17 °C. Figure 6a shows that the PM film contains microscale features as high as ~1 μm rising above a base with nanoscale features. For the latter type of features, Figure 6b presents a clearer representation to verify that the differences in height are below 200 nm. Both SEM and AFM images of the PM films show that its topography is rough on multiple scales, and as shown below, the rich topographic characteristics of the surface yield extreme behavior when the surface is in contact with water.

Surface Wettability. Table 2 shows the advancing (θ_A) and receding (θ_R) water contact angles for the same PM films grown for 24 h on HB+Au, HB+Ag/Au, and HB+Si and used in SEM characterizations. PM films on all substrates present advancing contact angles greater than 160° and differences between θ_A and θ_R, known as hysteresis, of 2°, 13°, and 39° for the HB+Au, HB+Ag/Au, and HB+Si surfaces, respectively. In the case of PM films grown from HB+Au, the film presents the characteristics of a superhydrophobic film ($\theta_A > 150°$, $\theta_A - \theta_R <$

(58) Snyder, R. G. *J. Mol. Spectrosc.* **1961**, *7*, 116–144.

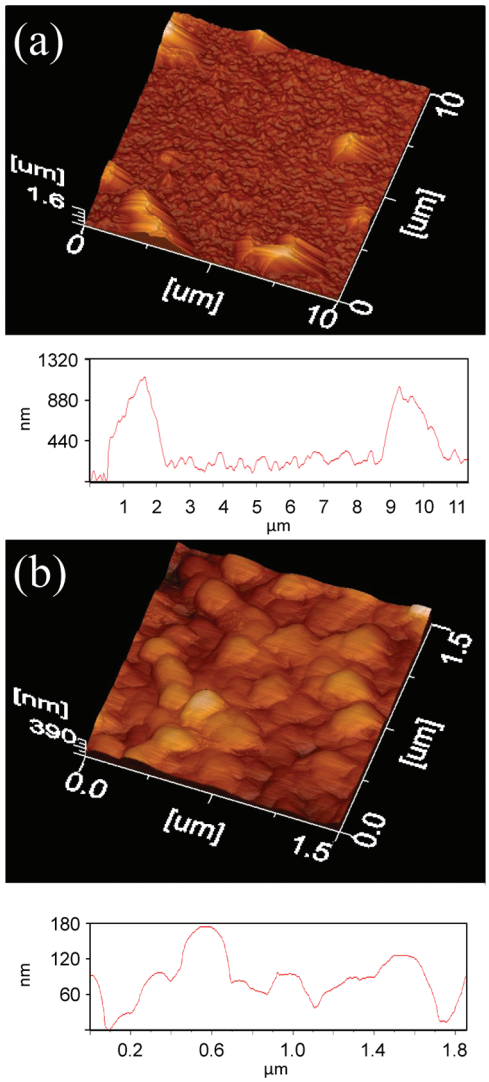

Figure 6. Tapping mode AFM images that show (a) microscale and (b) nanoscale features of PM films prepared by exposure of HB+Au to a 13 mM solution of DM in ether at −17 °C for 24 h. (b) Image acquired using a higher definition scan within the area of (a). Line scans represent the topographical features for a diagonal line across the image from the bottom left to the top right in the image.

Table 2. Water Contact Angles for PM Films Grown from HB+Au, HB+Ag/Au, and HB+Si Surfaces after 24 h of Polymerization in a 13 mM Solution of DM in Ether at −17 °C for 24 h

substrate	θ_A (deg)	θ_R (deg)
HB+Au	167 ± 2	165 ± 1
HB+Au/Ag	162 ± 3	149 ± 6
HB+Si	160 ± 2	121 ± 3

10°)[59,60] and enables impinging water drops to easily rebound from the surface without suffering noticeable shape deformation. HB+Ag/Au and HB+Si surfaces also present superhydrophobic behavior after 72 and 120 h of reaction, respectively, consistent with an increase in the number of microscale features as polymerization proceeds.

The behavior of the advancing contact angle (θ_A) for PM films grown from SIPM represents a substantial difference as compared to smooth PM surfaces (~103°).[14] Several authors[59,61,62] have shown that the film topography is responsible for the elevation of contact angles and the diminution of hysteresis, and surface roughness has been directly or indirectly included in the Wenzel and the Cassie contact angle models. In the Wenzel model[63−65] the water is assumed to wet the entire solid surface area, and the film topography of the surface is accounted by defining the roughness ratio (r),[59,63]

$$r = \frac{\text{actual area wetting the solid}}{\text{geometrical area}} \tag{2}$$

The predicted or Wenzel contact angle (θ_W) can be related to the contact angle on a smooth PM surface (θ_{PM}) by

$$\cos\theta_W = r\cos\theta_{PM} \tag{3}$$

In the Cassie model,[59,66−68] the water is assumed to not completely wet the solid surface area, enabling the presence of entrapped air in the grooves under the drop. Therefore, the composite interface is comprised of liquid−solid, liquid−air, and solid−air interfaces. In the Cassie model, the resulting contact angle (θ_C) is estimated as a contribution between the contact angle of the drop on a flat PM surface ($\theta_{PM} = 103°$) and the contact angle of the liquid in air ($\theta_{Air} = 180°$).

$$\cos\theta_C = \phi_{PM}(\cos\theta_{PM} + 1) - 1 \tag{4}$$

$$\phi_{PM} + \phi_{Air} = 1 \tag{5}$$

where ϕ_{PM} and ϕ_{Air} are the fractions of the projected area of the surface for polymer and air, respectively. The Cassie and Wenzel models are conceived as different wetting regimes.[64,65] Bico et al. proposed that both states are delimited by a critical roughness (r_c), in which surfaces with roughness ratios lower than r_c favor the formation of drops in the Wenzel state.[64]

$$r_c = \frac{\phi_{PM} - 1}{\cos\theta_{PM}} + \phi_{PM} \tag{6}$$

To analyze the wetting behavior of PM films grown by SIPM, we classify them depending on whether they follow the Cassie or the Wenzel state. Films in the Cassie state exhibit large contact angles and low hystereses,[59,60] which is the case for contact angles on PM films grown from HB+Au and HB+Ag/Au surfaces. For PM films grown from HB+Si, we observe that θ_A is similar to contact angles for PM films grown from HB+Au and HB+Ag/Au surfaces, and hence, the water drops advance in the Cassie state for all three films. For the case of θ_R for PM films grown from HB+Si, we first use eq 6 to calculate an r_c value of 2.9, assuming that $\phi_{PM} \ll 1$.[60] Then, we calculate the roughness ratio of the surface as 2.3 with eq 3, which, as compared[69] to r_c, suggests that after advancing in the Cassie state the drop collapses into the Wenzel state upon receding. After using eq 4 and the θ_R for PM films grown from

(59) Zhu, L. B.; Xiu, Y. H.; Xu, J. W.; Tamirisa, P. A.; Hess, D. W.; Wong, C. P. *Langmuir* **2005**, *21*, 11208–11212.
(60) Callies, M.; Quere, D. *Soft Matter* **2005**, *1*, 55–61.
(61) Nosonovsky, M. *Langmuir* **2007**, *23*, 3157–3161.
(62) Gao, L. C.; McCarthy, T. J. *Langmuir* **2006**, *22*, 2966–2967.
(63) Ulman, A. *Characterization of Organic Thin Films*; Butterworth-Heinemann: Boston, 1994.
(64) Bico, J.; Thiele, U.; Quéré, D. *Colloids Surf., A* **2002**, *206*, 41–46.
(65) Marmur, A. *Langmuir* **2003**, *19*, 8343–8348.
(66) Gao, L. C.; McCarthy, T. J. *Langmuir* **2006**, *22*, 6234–6237.
(67) Roach, P.; Shirtcliffe, N. J.; Newton, M. I. *Soft Matter* **2008**, *4*, 224–240.
(68) Bhushan, B.; Jung, Y. C. *Nanotechnology* **2006**, *17*, 2758–2772.
(69) Bittoun, E.; Marmur, A. *J. Adhes. Sci. Technol.* **2009**, *23*, 401–411.

Scheme 3. Equivalent Circuit Model Used to Represent Electrochemical Impedance Spectra for PM Films[a]

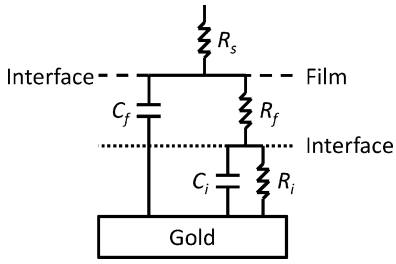

[a] Components of the circuit: R_s: resistance of the solution, C_i: capacitance of the interface, R_i: resistance of the interface, C_f: capacitance of the film, R_f: resistance of the film.

HB+Au and HB+Ag/Au surfaces, we estimate that less than 5% and 19%, respectively, of the area of the drop at the interface is in contact with PM.

The surface topography of the films influences the behavior of water droplets on the surface. Gao and McCarthy[62] showed that introduction of nanoscale roughness to an originally microscale rough surface decreased the surface hysteresis from 20° to ~0°. Here, we observe from SEM images that an increase in the concentration of microscale features (HB+Au > HB+Ag/Au > Si+Au) decreases hysteresis (HB+Au < HB+Ag/Au < Si+Au), thus increasing the stability of the drop in the Cassie state[59] and enabling the drops to easily rebound from the surface.[70] PM films grown from SIPM exhibit superhydrophobic behavior after times of polymerization that enable the growth of a sufficient number of micrometer-scale features that provide stability of the drops in the Cassie state, with times ranging from 24, 72, and 120 h for HB+Au, HB+Ag/Au, and HB+Si surfaces, respectively. In summary, these results suggest that SIPM enables the preparation of PM films with high contact angles (>150°) due to the pervasive presence of nanoscale ridges/valleys and that an increase of the isolated microscale features decreases hysteresis, enabling the preparation of superhydrophobic PM films.

Barrier Properties. The remarkable hydrophobic character of SIPM films due to the presence of air at the polymer/water interface opens the door to a diverse number of applications in which minimizing the contact between water and a substrate is critical. One of those applications is the protection of substrates using polymer coatings where the protective coating serves as a barrier to substances that can react and degrade the substrate interface. To investigate the effect that trapped air at the polymer/water interface has on the barrier properties against redox probes, we characterized PM films with electrochemical impedance spectroscopy (EIS) in the presence of 1 mM $K_3Fe(CN)_6$, 1 mM $K_4Fe(CN)_6 \cdot 3H_2O$, and 0.1 M Na_2SO_4(aq). EIS enables a comparison of the effective thickness and blocking properties of SIPM films (HB+Ag/Au, HB+Au) in relation to smoother PM films grown from non-polymethylenated surfaces (Au, Ag/Au, SAM+Ag/Au, SAM+Au) after 24 h of exposure to a 13 mM solution of DM at −17 °C. Comparison of the barrier properties depends on the ability to fit any resultant impedance spectrum to an equivalent circuit model composed of capacitors and resistors. Scheme 3 presents the general circuit model of a metal surface covered by a polymer film.[3,71] In this

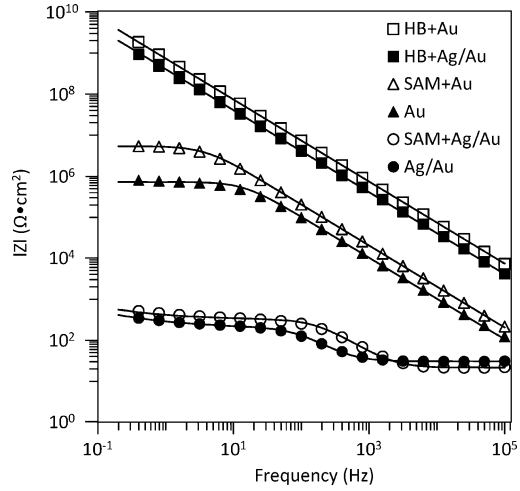

Figure 7. Electrochemical impedance spectra for PM films grown by exposure of various surfaces to a 13 mM solution of DM in ether at −17 °C for 24 h. Surfaces include two hydroborated SAMs, one on gold (HB+Au) and another on Ag/Au UPD (HB+Ag/Au), two vinyl-terminated SAMs not exposed to borane (SAM+Au, SAM+Ag/Au), as well as a Au and a Ag/Au surface. Solutions of 1 mM $K_3Fe(CN)_6$ and 1 mM $K_4Fe(CN)_6$ were used as soluble probes in a 0.1 M $NaSO_4$(aq) solution.

model, both the film and the organic/metal interface contribute to the total impedance. This model may be simplified on the basis of the relative values of each circuit component. For example, if the resistance of the film (R_f) is much larger than the interfacial impedance (defined as the parallel contribution of the interfacial capacitance (C_i) and resistance (R_i)), the spectrum will exhibit only a single time constant that is representative of the film (Randles model). Figure 7 shows a Bode plot of the experimental results with fits by a Randles[71] equivalent circuit model as solid lines. Table 3 lists the capacitance and resistance of the films that were quantified by fits to experimental data.

EIS results show that, after exposure to DM, Ag/Au surfaces (Ag/Au, SAM+Ag/Au) exhibit Warburg behavior (W) characteristic of uncoated metallic surfaces, indicating that little if any PM is grown on the surface.[72] In the case of Au surfaces (Au, SAM+Au), their exposure to DM enables the growth of PM films having impedance spectra that follow the Randles model and that exhibit well-defined resistances at low frequencies as the redox probes begin to penetrate the film. In contrast, films grown from the SIPM process show no signs of a resistive plateau ($R_f > 1 \times 10^{10}$ Ω•cm^2) at low frequencies but a linear increase of the log impedance with decreasing log frequency, with a slope of −1, reflecting ultrahigh impedance against the transfer of redox probes. Variation in the phase angle (ϕ) in the 10^{-1} to 10^5 frequency window for the same six substrates reported in Figure 7 (Figure S1 in Supporting Information) shows its balance between pure capacitive ($\phi = -\pi/2$) and pure resistive ($\phi = 0$) behavior and the higher sensitivity of ϕ versus $|Z|$ to measure breakdowns in the protection by the film.[73] The results agree with those of Figure 7, and more importantly, the fact that the superhydrophobic film grown from HB+Au displays a purely capacitive behavior ($\phi = -\pi/2$) for all frequencies indicates perfect barrier performance. The PM film grown from HB+Ag/Au (θ_A/θ_R = 162°/149°) shows a slight

(70) Chen, W.; Fadeev, A. Y.; Hsieh, M. C.; Oner, D.; Youngblood, J.; McCarthy, T. J. *Langmuir* **1999**, *15*, 3395–3399.
(71) Brantley, E. L.; Holmes, T. C.; Jennings, G. K. *J. Phys. Chem. B* **2004**, *108*, 16077–16084.
(72) Brantley, E. L.; Jennings, G. K. *Macromolecules* **2004**, *37*, 1476–1483.
(73) Bard, A.; Faulkner, L. *Electrochemical Methods*, 2nd ed.; John Wiley and Sons: New York, 2001.

Table 3. Film Resistance (R_f), Capacitance (C_f), and Thicknesses (d) for PM Films Grown from the Indicated Surfaces upon Exposure to a 13 mM Solution of DM in Ether at −17 °C for 24 h

	Ag/Au	SAM+Ag/Au	Au	SAM+Au	HB+Ag/Au	HB+Au
d (nm)[a]	6	1	228	315	3006	3554
R_f (Ω)			7.2×10^5	5.3×10^6	$>1 \times 10^{10}$	$>1 \times 10^{10}$
C_f (F)			1.6×10^{-8}	7.8×10^{-9}	3.9×10^{-10}	2.2×10^{-10}
R_i (Ω)	1.7×10^2	3.0×10^2				
C_i (F)	1.1×10^{-5}	3.3×10^{-6}				
W ($s^{1/2}/\Omega$)	3.6×10^{-3}	3.1×10^{-3}				

[a] Average thickness calculated from the values of Table 1.

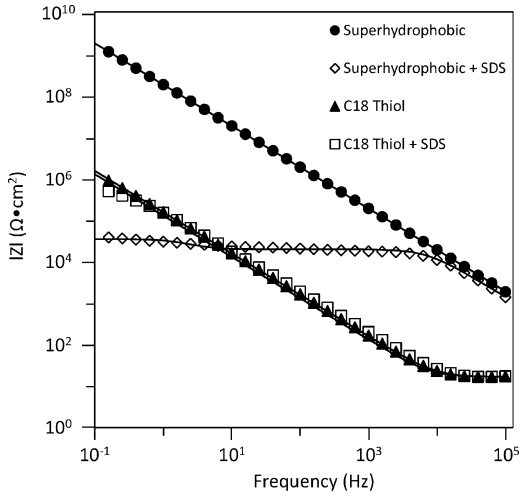

Figure 8. Change in the electrochemical impedance spectra for a superhydrophobic PM film (1.6 μm thick) grown from HB+Au after addition of SDS (∼16 mM) to the aqueous solution of 1 mM $K_3Fe(CN)_6$ and $K_4Fe(CN)_6$ and 0.1 M $NaSO_4$. A SAM on Au prepared from *n*-octadecanethiol both with and without surfactant served as a control.

increase in ϕ at low frequency, consistent with the onset of penetration by redox probes and highlighting the role of superhydrophobicity in the ability of the film to perfectly block redox probes from the substrate.

Tremendous differences in barrier properties between PM films grown from SIPM versus spontaneous DM polymerization could, at first sight, be attributed to differences in thickness. However, to determine the effect of superhydrophobicity on the barrier properties of PM films grown on Au from SIPM, we collected the impedance spectrum of a PM film under superhydrophobic and non-superhydrophobic conditions. To achieve superhydrophobic conditions, we used the aqueous redox solution mentioned above. For non-superhydrophobic conditions, we collected a new spectrum after decreasing the surface tension of the previous solution by adding sodium dodecyl sulfate (SDS, $2 \times \text{cmc} = 16$ mM).[74] Figure 8 shows a Bode magnitude plot of the resulting spectra and their fits as solid lines for a PM film grown from SIPM and, as a control, a SAM prepared from *n*-octadecanethiol both with and without surfactant. We selected a SAM as a control due to its molecularly smooth surface and inability to entrap much air at the organic/aqueous interface.

The superhydrophobic PM film behaves as an ideal capacitor that provides a defined separation of charge between the solution and the metal substrate due to the combined presence of air and PM as dielectric materials. However, addition of the surfactant breaks the superhydrophobic behavior,[74,75] favoring the displacement of the air in the grooves of the interface by the aqueous solution with reduced surface tension. This effect on the wetting properties ($\theta_{SDS} = 75 \pm 5°$ static contact angle of a ∼16 mM SDS(aq) solution on PM) results from the alteration of the interfacial tension of water after the surfactant molecules adsorb at the liquid−solid and liquid−gas interfaces.[76] The dramatic 10^5 Ω·cm^2 fold difference between these spectra at low frequencies (10^{-1} Hz) represents the magnitude of the superhydrophobic effect in maximizing the barrier properties. These results agree with those reported by Yin[77,78] and Liu,[79] in which high water contact angles (∼150°) of a surface coating correlated with reduced degradation of the metal substrate in the presence of corrosive environments. Here, however, for the first time, we have quantified the effect that superhydrophobicity has on the barrier properties as compared to non-superhydrophobic films of the same characteristics. In relation to the electrochemical behavior of SDS, Wang et al.[80] showed that organization of SDS at the interface decreases the passage of current in a cyclic voltammogram for a methyl-terminated SAM. To determine the implications of having SDS in solution, and as a manner of control, Figure 8 shows how the resultant spectra of a densely packed SAM before and after exposure to the surfactant exhibit little change in the electrochemical properties, suggesting that the substantial decrease in the barrier properties of the superhydrophobic film is not due to any electrochemical effect of the surfactant, but rather to the penetration of the solution through the grooves of the film. This argument is supported by the fact that the resistance for the PM film in the presence of SDS is lower than the resistance offered by the densely packed SAM that is only 2.5 nm thick. These results suggest that the PM film contains a topology that enables either the entrapment of air or the penetration of aqueous solution into the film when it is exposed to solutions of high or low surface tensions, respectively.

Conclusion

We have developed a new strategy to produce polymethylene films on gold and silicon surfaces by immobilizing borane on a vinyl-terminated monolayer, followed by its exposure to a DM solution in ether. This approach enables the control of film thickness by varying the time of polymerization or the DM concentration to produce PM films with superhydrophobic behavior and outstanding barrier properties. This methodology

(74) Mohammadi, R.; Wassink, J.; Amirfazli, A. *Langmuir* **2004**, *20*, 9657–9662.
(75) Ferrari, M.; Ravera, F.; Rao, S.; Liggieri, L. *Appl. Phys. Lett.* **2006**, 89.
(76) Feng-Ming, C.; Yu-Jane, S.; Hui, C.; Heng-Kwong, T. *Appl. Phys. Lett.* **2007**, *91*, 094108.
(77) Liu, T.; Chen, S.; Cheng, S.; Tian, J.; Chang, X.; Yin, Y. *Electrochim. Acta* **2007**, *52*, 8003–8007.
(78) Yin, Y. S.; Liu, T.; Chen, S. G.; Cheng, S. *Appl. Surf. Sci.* **2008**, *255*, 2978–2984.
(79) Liu, H. Q.; Szunerits, S.; Xu, W. G.; Boukherroub, R. *ACS Appl. Mater. Interfaces* **2009**, *1*, 1150–1153.
(80) Wang, J.; Zeng, B.; Fang, C.; Zhou, X. *J. Electroanal. Chem.* **2000**, *484*, 88–92.

of creating a superhydrophobic surface from an originally smooth surface has the versatility to be further extended to many other vinyl-terminated surfaces.

PM films grown from SIPM present a micrometer- and nanoscale morphology that is responsible for their superhydrophobic behavior. This morphology leads to entrapped air at the polymer/aqueous interface, which elevates both advancing and receding contact angles and enhances aqueous-phase barrier properties by orders of magnitude. This remarkable improvement in the barrier properties, combined with the precise control over film properties and the ability to generate superhydrophobic films, could open the door to a broad number of applications in which highly blocking surface coatings are required.

Acknowledgment. We gratefully acknowledge the National Science Foundation (CBET 0731168) for financial support of our work. N.N. acknowledges support from the Vanderbilt University School of Engineering Summer Undergraduate Research Experience Program.

Supporting Information Available: Experimental methods and a Bode phase plot that serves as a companion to Figure 7 are provided and discussed. This material is available free of charge via the Internet at http://pubs.acs.org.

JA9086193